TRPM7 is a molecular substrate of ATP-evoked P2X7-like currents in tumor cells

Wolfgang Nörenberg,[1]* Tanja Plötz,[1]* Helga Sobottka,[1] Vladimir Chubanov,[2] Lorenz Mittermeier,[2] Hermann Kalwa,[1] Achim Aigner,[1] and Michael Schaefer[1]

[1]Rudolf Boehm Institute of Pharmacology and Toxicology, Medical Faculty, Leipzig University, 04107 Leipzig, Germany
[2]Walther Straub Institute of Pharmacology and Toxicology, Ludwig Maximilian University of Munich, 80336 Munich, Germany

Within the ion channel–coupled purine receptor (P2X) family, P2X7 has gained particular interest because of its role in immune responses and in the growth control of several malignancies. Typical hallmarks of P2X7 are nonselective and noninactivating cation currents that are elicited by high concentrations (0.1–10 mM) of extracellular ATP. Here, we observe spurious ATP-induced currents in HEK293 cells that neither express P2X7 nor display ATP-induced Ca^{2+} influx or Yo-Pro-1 uptake. Although the biophysical properties of these ionic currents resemble those of P2X7 in terms of their reversal potential close to 0 mV, nonrectifying current-voltage relationship, current run-up during repeated ATP application, and augmentation in bath solutions containing low divalent cation (DIC) concentrations, they are poorly inhibited by established P2X7 antagonists. Because high ATP concentrations reduce the availability of DICs, these findings prompted us to ask whether other channel entities may become activated by our experimental regimen. Indeed, a bath solution with no added DICs yields similar currents and also a rapidly inactivating Na^+-selective conductance. We provide evidence that TRPM7 and ASIC1a (acid-sensing ion channel type Ia)-like channels account for these noninactivating and phasic current components, respectively. Furthermore, we find ATP-induced currents in rat C6 glioma cells, which lack functional P2X receptors but express TRPM7. Thus, the observation of an atypical P2X7-like conductance may be caused by the activation of TRPM7 by ATP, which scavenges free DICs and thereby releases TRPM7 from permeation block. Because TRPM7 has a critical role in controlling the intracellular Mg^{2+} homeostasis and regulating tumor growth, these data imply that the proposed role of P2X7 in C6 glioma cell proliferation deserves reevaluation.

INTRODUCTION

The extracellular signaling molecule ATP exerts its canonical actions via purinergic P2 receptors, comprising the ATP-gated nonselective channels P2X1-7, and G protein–coupled P2Y receptors $P2Y_1$-$P2Y_{13}$ (Jarvis and Khakh, 2009; Coddou et al., 2011; von Kügelgen and Harden, 2011). Within the P2X subfamily, P2X7 displays the lowest affinity for ATP and a marked allosteric inhibition by extracellular divalent cations (DICs; Yan et al., 2011). Upon repetitive or prolonged stimulation, P2X7 shows a run-up of current responses, and it allows a penetration of large cations, such as $NMDG^+$ or Yo-Pro-1, a process that has been associated with membrane blebbing and, eventually, apoptosis induction (reviewed in Coddou et al. [2011]). P2X7 is mainly expressed on immune cells, where it fuels inflammation by triggering interleukin-1β release. It is also expressed on a variety of cancer cells, where it has been suggested to either promote or suppress tumor progression (Di Virgilio, 2012).

During the characterization of allosteric P2X7 inhibitors, we realized that some modulators completely abrogated ATP-induced increases in $[Ca^{2+}]_i$ but only partially suppressed ATP-induced ionic currents under conditions that are typically applied in electrophysiological experiments with P2X7. To resolve this overt discrepancy, we tested the possibility that ATP had unexpectedly gated an additional, non–P2X7-associated background conductance. We found strong evidence for an as yet unrecognized activation of nonselective cation channels by ATP, closely resembling TRPM7 (melastatin-related transient receptor potential channel 7). This was unrelated to P2 receptor activation but most likely brought about by the release of these channels from a block by extracellular DICs, which are efficiently complexed by ATP when added at low millimolar concentrations that are typically required for P2X7 activation. As expected, the ubiquitously expressed TRPM7 (Fleig and Chubanov, 2014) was also present in the investigated tumor cell lines HEK293 and rat C6 glioma. The described mechanism should be considered when ascribing ATP-evoked cell responses to P2X7. TRPM7-like currents should also be taken into account when assessing the properties of P2X7 modulators especially under conditions of low extracellular cation concentrations. Future work will have to clarify whether high

*W. Nörenberg and T. Plötz contributed equally to this paper.
Correspondence to Michael Schaefer: michael.schaefer@medizin.uni-leipzig.de
Abbreviation used in this paper: DIC, divalent cation.

The Rockefeller University Press $30.00
J. Gen. Physiol. 2016 Vol. 147 No. 6 467–483
www.jgp.org/cgi/doi/10.1085/jgp.201611595

extracellular ATP concentrations, e.g., in cerebral ischemia or in cancer, may trigger pathophysiological responses via TRPM7 activation.

MATERIALS AND METHODS

Materials and compounds

The P2X7 antagonists A-438079, A-839977, and AZ-10606120 were from Tocris Bioscience. Unless otherwise stated, all other chemicals were from Sigma-Aldrich. Stock solutions of drugs were prepared in standard or low-DIC bath solutions (ATP disodium salt, TNP-ATP [2′,3′-O-(2,4,6-trinitrophenyl) adenosine 5′-triphosphate] sodium salt), distilled water (BBG [Coomassie brilliant blue G-250], suramin), or DMSO (A-438079, A-839977, AZ-10606120, amiloride, NS-8593). Aliquots of stock solutions were stored at −20°C, and freshly diluted at the day of the experiment. The DMSO concentration in bath solutions never exceeded 0.1%, a concentration that had no effects on ATP-induced currents, Ca^{2+} entry signals, and Yo-Pro-1 uptake responses in HEK_{hP2X7} cells. ATP stock solutions were routinely readjusted to pH 7.3 with NaOH.

Cell culture

Parental and stably transfected HEK293 cells, expressing the human P2X7 (HEK_{hP2X7}), were cultured at 37°C and 5% CO_2 in Dulbecco's modified Eagle medium (DMEM; c.c.pro), containing 4.5 mM D-glucose, 10% FCS (Biochrom), 2 mM L-glutamine (PAA), and 0.05 mg/ml geneticin (Invitrogen). HEK293 cells (#CRL-1573; ATCC) were used in passages 8–26 after purchase; stable transfection was performed on cells in passage 11. Rat C6 glioma cells were obtained from the German Collection of Microorganisms and Cell Cultures (DSMZ; lot #3) and cultured for up to 20 passages in DMEM with 4.5 mM D-glucose, 10% FCS, L-glutamine, and sodium bicarbonate (DMEM; Sigma-Aldrich).

Intracellular [Ca^{2+}] analysis

$[Ca^{2+}]_i$ analysis in suspensions of HEK293, HEK_{hP2X7}, or rat C6 glioma cells was conducted in a fluorescence imaging plate reader essentially as described previously (Nörenberg et al., 2012) with the following modifications: fluo-4/AM–loaded cells were resuspended in HEPES-buffered saline (HBS), containing 130 mM NaCl, 6 mM KCl, 1 mM $CaCl_2$, 1 mM $MgCl_2$, 5.5 mM D-glucose, and 10 mM HEPES (pH 7.4 with NaOH). Cells were dispensed into 384-well plates and exposed to the indicated modulators for 15 min. Fluorescence intensities were monitored during application of ATP. Unless otherwise stated, the final concentration of ATP was 1 mM. Background signal–corrected fluorescence intensities were normalized to the initial intensities (F_0) to compensate for uneven loading and fluorescence detection sensitivity.

YO-PRO-1 uptake assay

HEK cell lines and rat C6 glioma cells were grown to confluent monolayers in 25-cm^2 cell culture flasks, harvested with trypsin, and resuspended in a modified HBS buffer, containing low DIC concentrations (no $MgCl_2$ and 0.1 mM $CaCl_2$; low DIC). 1 µM YO-PRO-1 (Thermo Fisher Scientific) was added to the cell suspension before dispensing it into 384-well microtiter plates prefilled with ATP. Experiments were conducted in a fluorescence imaging plate reader setup (Nörenberg et al., 2012).

Western blot analysis

To study expression levels of native TRPM7, we subjected whole-cell lysates or membrane fractions of HEK293 or rat C6 glioma cells to SDS-PAGE (7% acrylamide/bis-acrylamide), electroblotted the proteins on nitrocellulose membranes, and probed the membranes after blocking with 5% (wt/vol) nonfat dry milk and 0.1% Tween 20 in phosphate-buffered saline (PBST) with recombinant rabbit monoclonal EPR4582 antibody (1:3,000; Abcam), followed by washing in PBST and incubation with horseradish peroxidase–coupled anti–rabbit IgG (1:1,000; Cell Signaling Technology) and washed again in PBST. Blots were exposed in a luminescence imager (Peqlab/VWR). As a positive control, mouse TRPM7-encoding plasmids were transiently transfected in HEK293 cells. Membrane fractions were obtained by repeatedly aspirating cell suspensions through a 0.45-mm needle, followed by pelleting at 13,000 rpm for 20 min at 4°C.

To detect P2X7 and β-actin expression, HEK293 cells or C6 glioma cells were washed with phosphate-buffered saline (PBS) and triturated (aspiration through 0.45-mm needle) in a lysis buffer, pH 7.4, containing 8 M urea, 10 mM TRIS, and 10 mM NaH_2PO_4. Aliquots were separated by SDS-PAGE (12.5%) and electroblotted on nitrocellulose membranes (0.45 µm; Bio-Rad Laboratories). Blots were cut at a position corresponding to 55 kD and probed with either anti-P2X7 (1:1,000; Alomone Labs; upper part of the blot) or anti–β-actin (1:3,300; Sigma-Aldrich; lower part of the blot) at 4°C overnight. After washing with PBST, blots were incubated with horseradish peroxidase–coupled goat anti–rabbit IgG (1:2,000; Thermo Fisher Scientific) and washed again. Bioluminescence detection was performed using a chemiluminescence kit (ECL; Thermo Fisher Scientific) and a cooled charge-coupled device camera (QSI540; Quantum Scientific Imaging).

Electrophysiology

Whole-cell or outside-out patch-clamp recordings were performed at 20–25°C and, unless otherwise stated, at a holding potential of −60 mV using an EPC9 amplifier controlled by Pulse software (HEKA). The extracellular solution contained 147 mM NaCl, 2 mM KCl,

13 mM D-glucose, and 10 mM HEPES (~305 mOsm/l; pH 7.3 with NaOH), supplemented with 1 mM $MgCl_2$ and 2 mM $CaCl_2$ (standard DIC) or with only 0.1 mM $CaCl_2$ (low DIC). A DIC-free bath (no DIC) was produced by omitting Ca^{2+} and Mg^{2+} and supplementing EGTA and EDTA (1 mM each) to remove any contamination with free DICs. Other extracellular solutions with a defined free [Ca^{2+}] were prepared by adding the required amounts of Ca^{2+} to the no-DIC solution as calculated with a MaxChelator software. Patch pipettes had a resistance of 2–5 MΩ, when filled with intracellular solutions. These were either identical with the no-DIC saline (outside-out patches) or contained 147 mM KCl, 10 mM HEPES, 10 mM EGTA (~300 mOsm/l; pH 7.3 with KOH; whole-cell configuration). In some experiments, 3 mM of $MgCl_2$ (MaxChelator) was added to either of the two pipette solutions. Drugs were applied to patched cells by means of a pressurized superfusion system (OCTAFLOW-II; ALA Scientific Instruments). Whole-cell currents (filtered at 1.7 kHz, sampled at 5 kHz) were measured as peak amplitudes and normalized for membrane capacitance to obtain current densities (pA/pF). Experiments during which series resistance (compensated by 60–80%) changed by >20% were discarded. Single-channel currents from outside-out patches were digitized at 20 kHz and filtered at 2 kHz.

Data evaluation and statistical analysis

ATP concentration-response curves were obtained by fitting the experimental data to a Hill equation: $E = E_{min} + (E_{max} - E_{min})/(1 + ([M]/EC_{50})^{-nH})$, where E_{min} and E_{max} are the extrapolated minimum and maximum effects, $[M]$ is the actual concentration, EC_{50} is the activator concentration producing 50% of the response, and nH is the Hill coefficient, indicating the cooperativity of the effect.

Single channel data stem from recordings, in which no overlapping events were observed. Channel openings were grouped in burst of variable duration, which were separated by long (>200 ms) closed states. Being beyond the scope of the present study, this kinetic behavior was not explored further. Analysis of channel lifetimes and open probabilities was therefore restricted to visually identified bursts.

Baseline correction, if necessary, artifact removal, and idealization of single channel raw data were performed with the QUB program. The unitary current amplitude was determined from all-points amplitude histograms that were fitted to the sum of two Gaussian distributions. The single channel chord conductance was calculated thereof, assuming a reversal potential of 0 mV, and the associated relative excess open channel noise (σ_{ex}/i) was derived from the root mean square difference between the variances of the open and closed channel current. Referred open probabilities (P_O) were computed from the ratio of the area of the open channel to the total area of the amplitude histogram.

Event sequence detection for intraburst channel lifetime analysis was performed via a recursive Viterbi algorithm (segmental k-means algorithm [SKM]) implemented in QUB and by using a simple two-state (closed ↔ open) model. The dead time imposed (~1.2-fold of the filter rise time; Qin, 2004) was 200 µs, thereby excluding events shorter than this duration from analysis. The SKM approach has, because of a high tolerance for noise, a low tendency for false event recognition, and its accuracy is in addition largely insensitive to the kinetic model, i.e., to the number of states and/or the initial rate constants used (Qin, 2004). The mean intraburst closed (T_C) and open times (T_O) given were averages derived from the noise-free idealization. SKM-derived dwell times were additionally displayed as histograms of square root–transformed, log-distributed data and overlaid with theoretical distributions (probability density functions) to provide a supplementary visual check for multiple peaks (i.e., kinetic components; Sigworth and Sine, 1987; for examples see Fig. 5 [C and D]).

All data were expressed as mean ± SEM, obtained in n cells or experiments. Differences in means were tested for significance by the Mann-Whitney U test or by the Kruskal-Wallis one-way ANOVA on Ranks followed by a modified Student's t test (Bonferroni-Dunn) in the case of single and multiple comparisons, respectively. P-values are stated in the figures and in the text.

Online supplemental material

Fig. S1 shows transient currents evoked by DIC-free bath solutions (no DIC) are amiloride sensitive and inhibited by ATP. Fig. S2 shows voltage dependence of TRPM7 block by ATP in low DIC and in the presence of 2.4 µM $[Ca^{2+}]_o$. Fig. S3 shows knockdown of TRPM7, but not P2X7, suppresses sustained no-DIC–induced current in HEK_{hP2X7} cells. Fig. S4 shows ATP evokes TRPM7-like currents in the presence of standard extracellular DIC concentrations. The supplemental text shows that transient ASIC1a (acid-sensing ion channel type Ia)-like currents are induced by low $[Ca^{2+}]_o$ in HEK_{hP2X7} cells. Online supplemental material is available at http://www.jgp.org/cgi/content/full/jgp.201611595/DC1.

RESULTS

An atypical, P2X7 receptor–like background conductance in HEK_{hP2X7} and parental HEK293 cells

In a stably transfected, P2X7-expressing cell line (HEK_{hP2X7}), whole-cell currents elicited by 1 mM ATP were largely, but not completely inhibited by a combination of a broad-spectrum P2X receptor blocker (30 µM TNP-ATP) and a P2X7-specific antagonist (0.3 µM AZ-10606120; Fig. 1 A). When subjecting the parental HEK293 cell line, which is not expected to

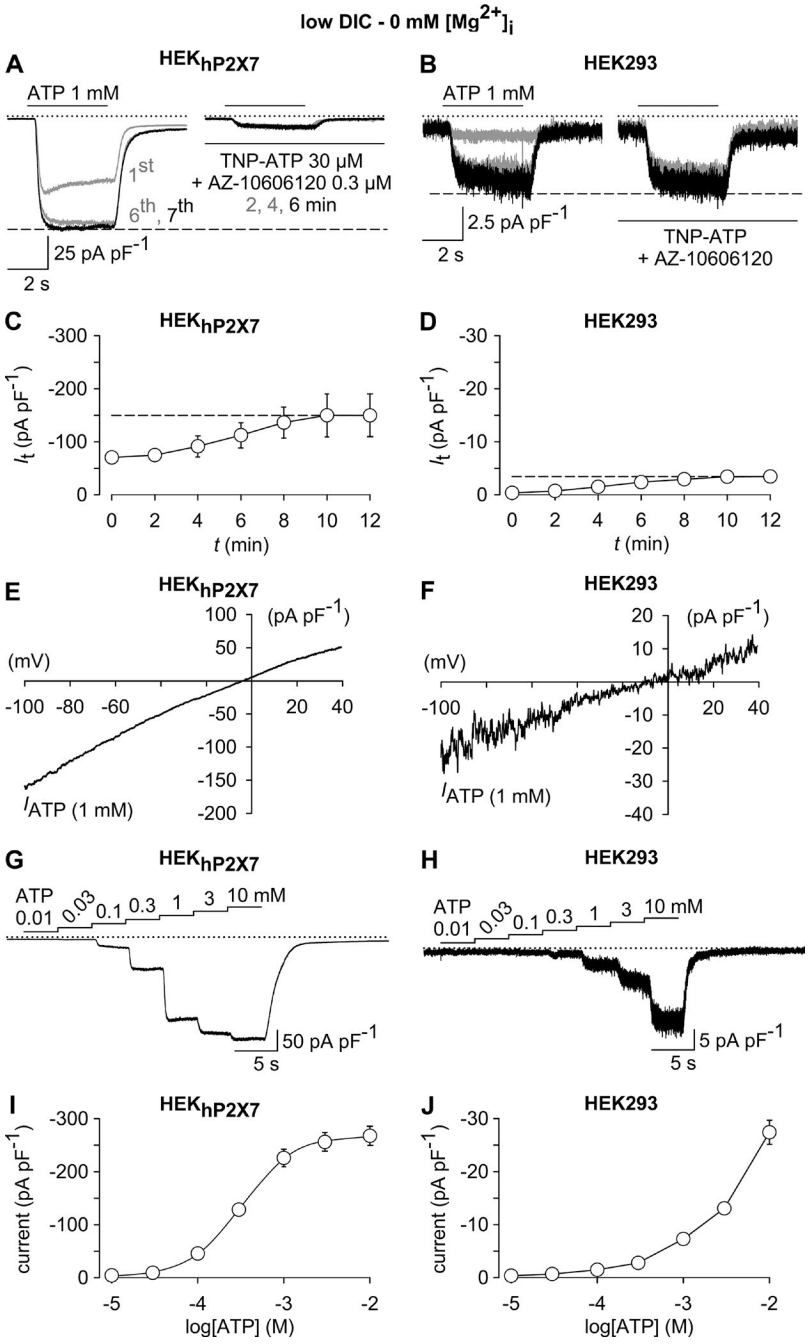

Figure 1. **Similarities and dissimilarities between ATP-induced whole-cell currents in HEK$_{hP2X7}$ and HEK293 cells.** (A and B) Superimposed whole-cell currents obtained in HEK$_{hP2X7}$ (A) or HEK293 cells (B) in response to 1 mM ATP during preconditioning (left) and after 2, 4, and 6 min in the presence of a P2X receptor–blocking mixture of TPNP-ATP (30 µM) and AZ-10606120 (0.3 µM; right). Note the only partial inhibition by the antagonist cocktail in HEK$_{hP2X7}$ cells, as well as the insensitivity of ATP-responses in HEK293 cells. (C and D) Statistical evaluation of the preconditioning phase in experiments similar to those in A and B, showing a comparable amplitude run-up in HEK$_{hP2X7}$ (C) and HEK293 cells (D; n = 7 each). (E and F) I/V relationship of net ATP (1 mM)-induced currents (I_{ATP}) in HEK$_{hP2X7}$ (E) and HEK293 cells (F) showing an almost linear behavior over the voltage range tested (−100 to 40 mV), as well as a reversal potential close to 0 mV for both cell lines. (G–J) Representative whole-cell currents (G and H) and their statistical evaluation (I and J), showing ATP concentration-response curves in HEK$_{hP2X7}$ (G and I) and HEK293 cells (H and J; n = 11 each). The EC_{50} value and the Hill slope derived from the HEK$_{hP2X7}$ cell responses were 339 ± 27 µM and 1.7 ± 0.2, respectively. All recordings were performed in a low-DIC bath, using a Mg^{2+}-free pipette solution, and cells were at first repetitively stimulated for 4-s and at 120-s intervals (preconditioning) with 1 mM (A–F) or 10 mM ATP (G–J; not depicted) until current run-up was completed. I_{ATP} in E and F was obtained by digitally subtracting responses to 1-s voltage ramps imposed in the absence of ATP from those recorded in the presence of the activator. ATP concentration-response curves (G–J) were constructed from responses to subsequent 4-s challenges with stepwise increasing concentrations of the agonist. In electrophysiological figures, dotted lines indicate the zero current level. Error bars indicate SEM.

express P2X7, to the same protocol, 1 mM ATP also induced inward currents (Fig. 1 B). These spurious currents were smaller in size and not sensitive to the combined application of TNP-ATP and AZ-10606120 (Fig. 1 B). Nonetheless, they shared some properties that are typical for a P2X7-like conductance, including a noninactivating phenotype, a current run-up during repeated pulses of ATP application (Fig. 1, C and D), an almost linear I/V relationship with a reversal potential close to 0 mV (−3.8 ± 0.6 mV in HEK$_{hP2X7}$ cells vs. −3.6 ± 0.9 mV in parental HEK293 cells; Fig. 1, E and F), and a requirement of high ATP concentrations for current activation (Fig. 1, G–J). With a lack of a saturating effect at ATP concentrations of 1–10 mM, the concentration dependence of ion currents in parental HEK293 cells seemed to differ from that seen in the HEK$_{hP2X7}$ cell line.

Because neither Ca^{2+} entry nor Yo-Pro-1 uptake were detectable in ATP (1–5 mM)-stimulated parental HEK293 cells (not depicted) and because endogenous $P2Y_1$ and $P2Y_2$ receptors in HEK293 cells are unlikely to require more than 10 µM ATP for activation, we considered that these background currents may be unrelated to P2 receptors in general. We therefore aimed at clarifying the molecular correlate of these unexpected ATP-induced background currents.

Drops to low $[Ca^{2+}]_o$ evoke two types of current responses in HEK_{hP2X7} cells

To explore the possibility that millimolar concentrations of ATP may complex a substantial fraction of DICs in the bath solution and thereby release yet to be identified channels from a DIC block, we exposed HEK_{hP2X7} cells to bath solutions that contained the same calculated free Ca^{2+} concentrations that would remain in low-DIC bath solutions, supplemented with 0.1–10 mM ATP (Fig. 2 A). To this end, HEK_{hP2X7} cells were kept in standard DIC and then acutely exposed to test solutions with stepwise decrements of $[Ca^{2+}]_o$ to 100 µM Ca^{2+} (low DIC) or 76.5, 21.3, or 2.4 µM free Ca^{2+}, corresponding to the calculated concentrations upon addition of 0, 0.1, 1, and 10 mM ATP to low-DIC bath solutions. In addition, a Ca^{2+}-free solution (no DIC) was applied. Under these conditions, we observed two current components, which both displayed an inverse $[Ca^{2+}]_o$ concentration dependence. A transient inward current component was seen at $[Ca^{2+}]_o \leq 76.5$ µM and partially deactivated during repeated application of the Ca^{2+}-depleted solutions (Fig. 2, B–F and H). In contrast, a more P2X7-like sustained current component developed upon repetitive stimulation with an amplitude run-up (Fig. 2 G), thus indicating a similar behavior to that seen in ATP-challenged HEK293 cells. The transient and sustained responses differed in their $[Ca^{2+}]_o$ sensitivity (Fig. 2 I), indicating that they are conducted by distinct channel entities. The transient inward currents were sensitive to 10 µM amiloride (Fig. S1) and are presumably carried by ASIC1a channels known to be expressed in HEK293 cells (Gunthorpe et al., 2001) and to shift their pH dependence to more neutral values in a $[Ca^{2+}]_o$-dependent manner (Babini et al., 2002; Sherwood et al., 2012). A more detailed description is provided in the Supplemental text. Notably, the amplitudes of the noninactivating currents evoked by acutely lowering $[Ca^{2+}]_o$ in HEK_{hP2X7} cells matched fairly well those of the ATP-induced currents in parental HEK293 cells (Fig. 2 I) or of TNP-ATP– and AZ-10606120–resistant residual currents that remained in ATP-stimulated HEK_{hP2X7} cells (Fig. 1 A), suggesting that the ATP-induced background current may be present in both cell lines and is only indirectly triggered by chelation of extracellular DICs.

Noninactivating whole-cell currents induced by ATP or by low $[Ca^{2+}]_o$ share regulatory properties with TRPM7

We first wanted to know which channel may mediate currents that were triggered by lowering $[Ca^{2+}]_o$. During application of slow voltage ramps, outwardly rectifying currents were evident in HEK293 cells (not depicted) or in HEK_{hP2X7} cells patched with a Mg^{2+}-free pipette solution in the presence of extracellular DICs (Fig. 3, A and B). After changing to no-DIC solution, inward and outward currents strongly increased, associated with a linearization of the I/V relationship, which reversed at −6.0 ± 1.6 mV (n = 10; Fig. 3, A and B). These features are most likely caused by the same channel, which is released from a voltage-dependent inhibition by extracellular DICs and closely resemble the properties of the poorly selective and Mg^{2+}-inhibited cation channel TRPM7 (Nadler et al., 2001), which is widely expressed in untransformed or in tumor cells, including HEK293 (Chubanov et al., 2004). Western blot analysis confirmed the TRPM7 expression in parental HEK293 and in HEK_{hP2X7} cell lines (Fig. 3 C). If TRPM7 was the activated channel, we would expect a strong suppression by intracellular Mg^{2+}. Indeed, including 3 mM $MgCl_2$ in the pipette solution abrogated the sustained current component that was induced by a Ca^{2+}-free bath solution (Fig. 3, D and F). Instead, the transient inward currents that were still inducible by removing $[Ca^{2+}]_o$ now became unmasked and isolated (Fig. 3, E and G). Of note, the transient current component was inwardly rectifying and reversed at >40 mV, strongly indicating a Na^+-selective conductance.

Because the ATP-induced background current, which remained in the presence of TNP-ATP and AZ-10606120, was also abolished by including 3 mM $MgCl_2$ in the pipette solution (Fig. 4, A–C), it appeared likely that this background current is caused by an activation of TRPM7. Consistently, 30 µM NS-8593, a compound that has previously been shown to inhibit TRPM7 (Chubanov et al., 2012), caused a reduction of current densities (Fig. 4, D and E). We conclude that TRPM7 may mediate ATP-induced background currents that appear under conditions that are frequently applied to analyze P2X7. To confirm that TRPM7 is the molecular correlate, the biophysical fingerprint of TRPM7, favorably by single channel analysis, would have to be assessed.

ATP- and low $[Ca^{2+}]_o$–activated single channel currents are virtually undistinguishable and resemble TRPM7

If TRPM7 was the channel that is activated by chelation or removal of extracellular DIC, we would expect to observe a single channel conductance of ∼40 pS (Li et al., 2006). Because the unitary conductance of P2X7 is 9–10 pS (Riedel et al., 2007), single channel analysis should yield a distinction between these channel entities. Outside-out patches were obtained from nontransfected HEK293 cells and voltage clamped to −60 mV in a bath solution containing standard DIC. After reaching stable seals (2–10 min), patches were exposed to no-DIC bath solution, which gave rise to bursts of channel activity in 14 out of 18 patches. In 8 out of 14 channel-containing patches, a single open level was seen (Fig. 5 A). Amplitude histograms revealed a unitary conductance of 41.2 ± 1.5 pS, indicating TRPM7 activity. When challenged with 10 mM ATP in low-DIC solution (inducing a calculated $[Ca^{2+}]_o$ of 2.4 µM), again single channel activity appeared in 8 out of 14 patches,

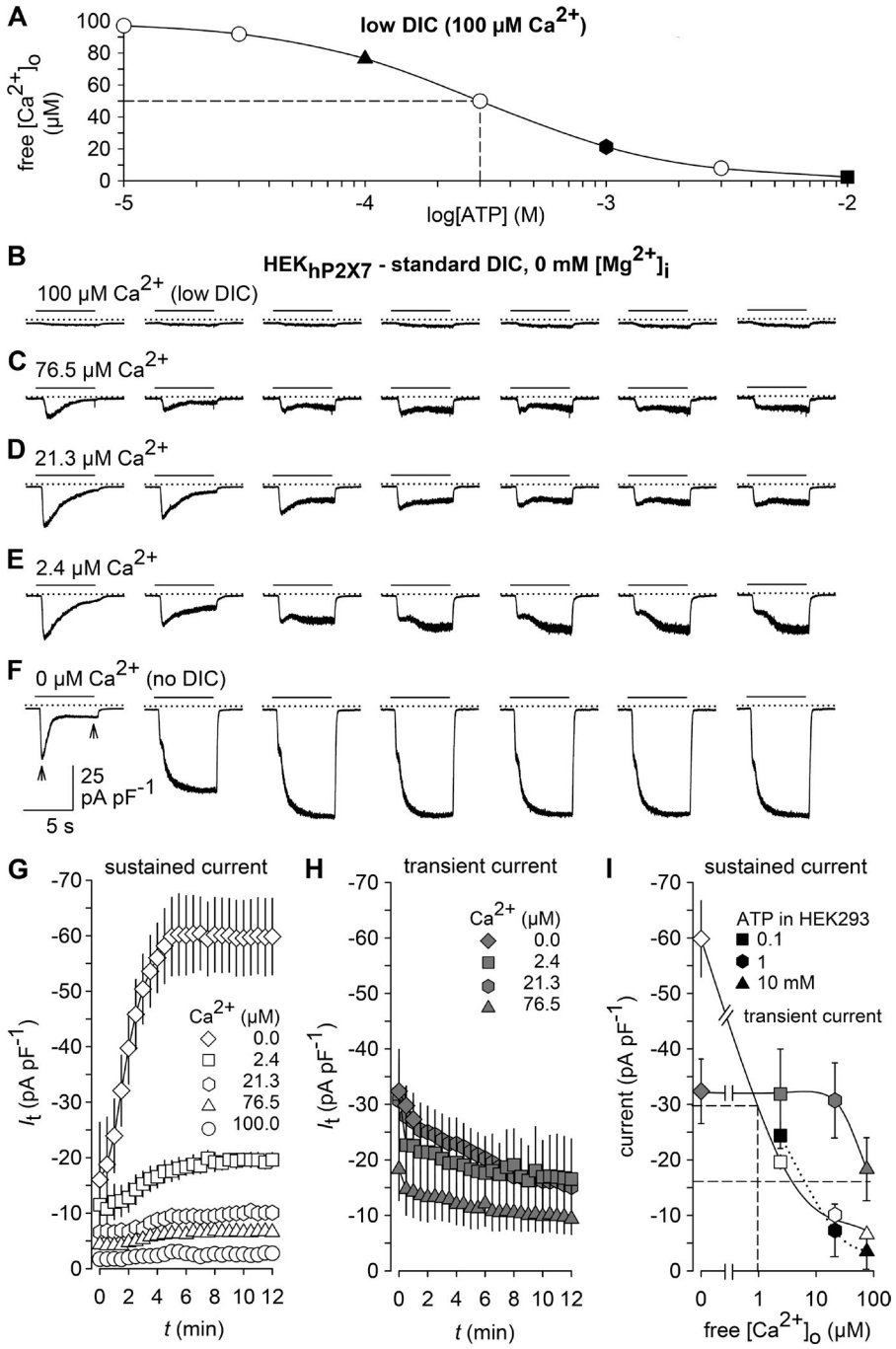

Figure 2. **Effects of $[Ca^{2+}]_o$ on membrane conductance.** (A) Calculated free Ca^{2+} concentration in a bath containing 100 μM Ca^{2+} (low DIC) and variable concentrations of ATP. Filled symbols indicate solutions with Ca^{2+} concentrations used for stimulation in C–E. (B and F) Typical patterns of membrane currents in response to the indicated acute drops in $[Ca^{2+}]_o$, caused by bath solutions, in which the indicated free $[Ca^{2+}]_o$ was adjusted by buffering with EGTA and EDTA instead of ATP. Responses in C–E correspond to the theoretical Ca^{2+}-lowering effect of 0.1, 1, and 10 mM ATP, respectively. Note that only every fourth response is shown for clarity. (G and H) Statistical evaluation of experiments similar to those in B–F (n = 10 each). The amplitudes of the sustained (G) and the transient current components (H) in response to lowered $[Ca^{2+}]_o$ were measured, as indicated by the arrows in the left panel of F, at the end of the stimulation and at the peak response, respectively. (I) Concentration-dependent effects of bath Ca^{2+} on membrane conductance. Apparent IC_{50} values (broken drop lines) were ~1 μM Ca^{2+} for the sustained current and >76.5 μM Ca^{2+} for the transient current. Curves for the sustained (open symbols) and transient current component (gray symbols) were constructed from the maximum responses in G and H. Current amplitudes evoked by 0.1, 1, and 10 mM ATP in P2X receptor–devoid HEK293 cells (black symbols) are replotted from Fig. 1 J for comparison. Recordings were performed in a standard DIC bath, using a Mg^{2+}-free pipette solution, and cells were repetitively stimulated for 6 s at 30-s intervals with bath solutions of the indicated Ca^{2+} content. In electrophysiological figures, dotted lines indicate the zero current level. Error bars indicate SEM.

but with markedly shorter opening events and an apparent unitary conductance of 25.8 ± 0.7 pS (Fig. 5 B). If 3 mM $MgCl_2$ was included in the pipette solution, neither removal of extracellular DIC nor exposure to ATP induced a single channel activity (n = 7 for each setting; not depicted), arguing for the $[Mg^{2+}]_i$-inhibited TRPM7 channel as the common molecular correlate. The overt dissimilarities between single channel properties elicited by no-DIC solution or by 10 mM ATP in low DIC, however, prevent the unequivocal assignment of TRPM7 being the channel, which is indirectly activated by ATP. The calculated mean open times during activity bursts were 49.4 ± 5.8 ms and 2.7 ± 0.8 ms for single channel openings induced by no DIC and ATP, respectively ($P < 0.001$, n = 8; Fig. 5, C–E). Other significant differences were the lower apparent intraburst open probability, smaller unitary current amplitudes, and notably, an ~1.5-fold higher excess open channel noise (σ_{ex}/i) upon ATP-induced compared with low-DIC–mediated currents (Fig. 5 E). The increased excess channel noise indicates a possible underestimation of the single channel conductance, caused by a fast block of the channel in the ATP-activated mode, which cannot be resolved within the methodological restrictions imposed by the

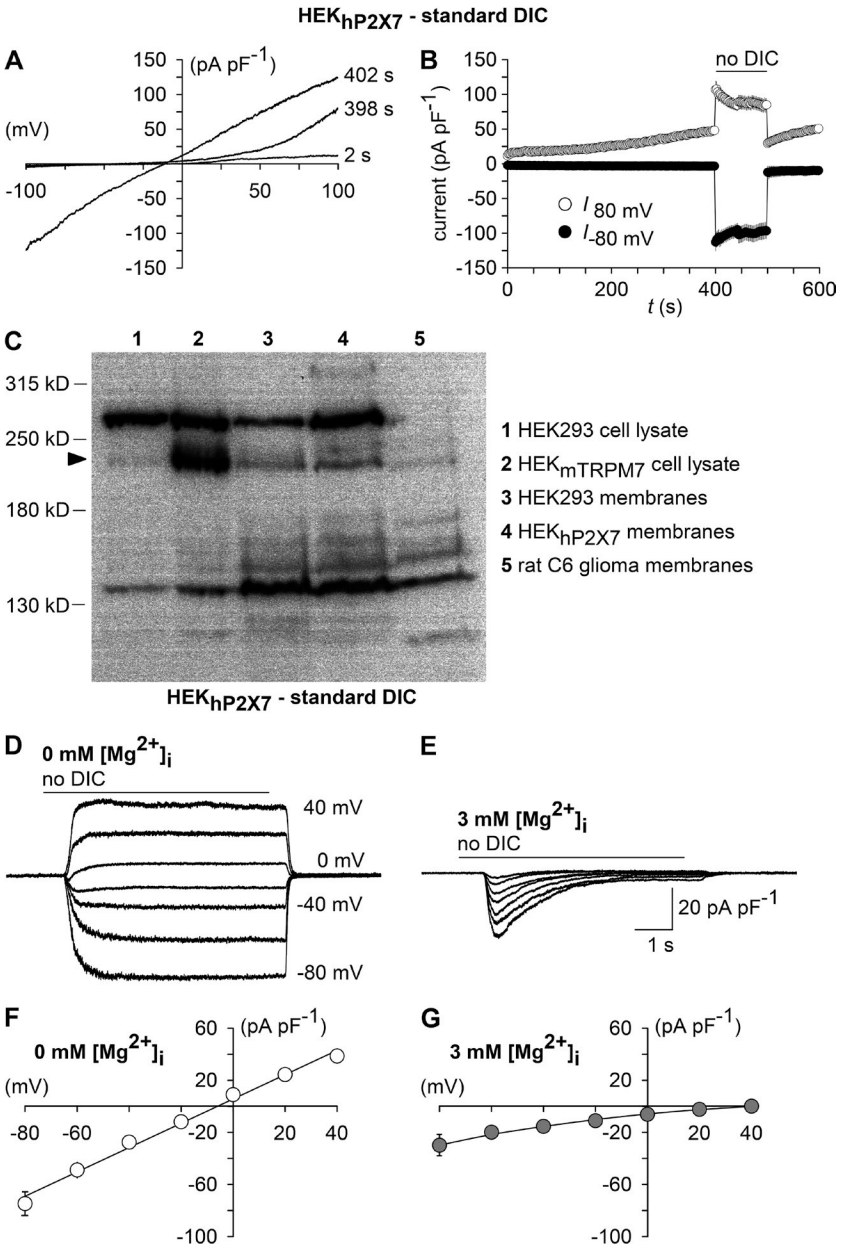

Figure 3. **TRPM7 fingerprinting.** (A) Shown are superimposed currents in a HEK_{hP2X7} cell during application of voltage ramps (0.8 mV/ms) under standard DIC conditions at 2 and 398 s after the start of the experiment and, additionally, at 402 s, when the extracellular medium had been exchanged to no DIC. The holding potential between ramps was 0 mV. (B) Statistical evaluation of seven experiments performed as shown in A. Depicted are inward current amplitudes at −80 mV (filled circles) and outward current amplitudes at 80 mV (open circles) versus time. Note the run-up of outward currents, as well as the augmentation of inward currents associated with a linearization of the previously outwardly rectifying I/V curve in the absence of extracellular DICs (no DIC), which are characteristic features of TRPM7. (C) Western blot analysis of TRPM7 expression in membrane fractions of parental HEK293 cells (3), HEK_{hP2X7} cells (4), and rat C6 glioma cells (5). Blots were probed with recombinant monoclonal anti-TRPM7.Whole-cell lysates of HEK293 cells transiently transfected with an expression plasmid encoding mouse TRPM7 (HEK_{mTRPM7}, 2) were used to visualize the position of the TRPM7-specific band (arrowhead), and results from the respective untransfected HEK293 clone 1 are shown for comparison. (D and E) Superimposed whole-cell currents from HEK_{hP2X7} cells recorded with a Mg^{2+}-free (D) or 3 mM Mg^{2+}–containing pipette solution (E), showing the effect of no-DIC bath, which was repeatedly applied 6 s at 30-s intervals at varying (20-mV increments) membrane voltages. Note that sustained responses were abolished by 3 mM $[Mg^{2+}]_i$. (F and G) Current-voltage curves constructed from experiments similar to those in D and E (n = 11 each). Error bars indicate SEM.

applied filtering and sampling frequencies. Because shorter mean open times are not explained by this fast block, the ATP-activated conductance may be caused either by a different channel or by TRPM7, whose openings are modulated by a combined action of a fast and a slower, flickering block.

If distinct kinetic properties can be adopted by the same channel, we would expect that, in an excised patch with a single level of channel openings, acute switching from one to the other activation mode should demonstrate that these features reflect interconvertible states of a single channel. In outside-out patches exposed to 10 mM ATP in low DIC, the aforementioned flicker channel activity was observed and, upon switching to no DIC, successively converted into the more stabilized openings (Fig. 6 A). Switching back to ATP in low DIC immediately reestablished the channel flickering. During this procedure, the apparent single channel conductance also converted from ~25 pS to 40 pS and back to 25 pS. Because similar reversible conversion of single channel properties was achieved with ATP included in the no-DIC solution (Fig. 6, B and D), we conclude that the ATP itself does not account for the kinetic changes but may act via incomplete chelation of $[Ca^{2+}]_o$. This assumption was corroborated by applying an ATP-free extracellular solution, but with $[Ca^{2+}]_o$ adjusted to 2.4 μM. Again, a flickering channel activity with lower apparent amplitudes was observed, which converted to longer openings with a higher unitary conductance after removal of the remaining $[Ca^{2+}]_o$ (Fig. 6, C and D). As a second line of evidence, we could demonstrate that the ATP-

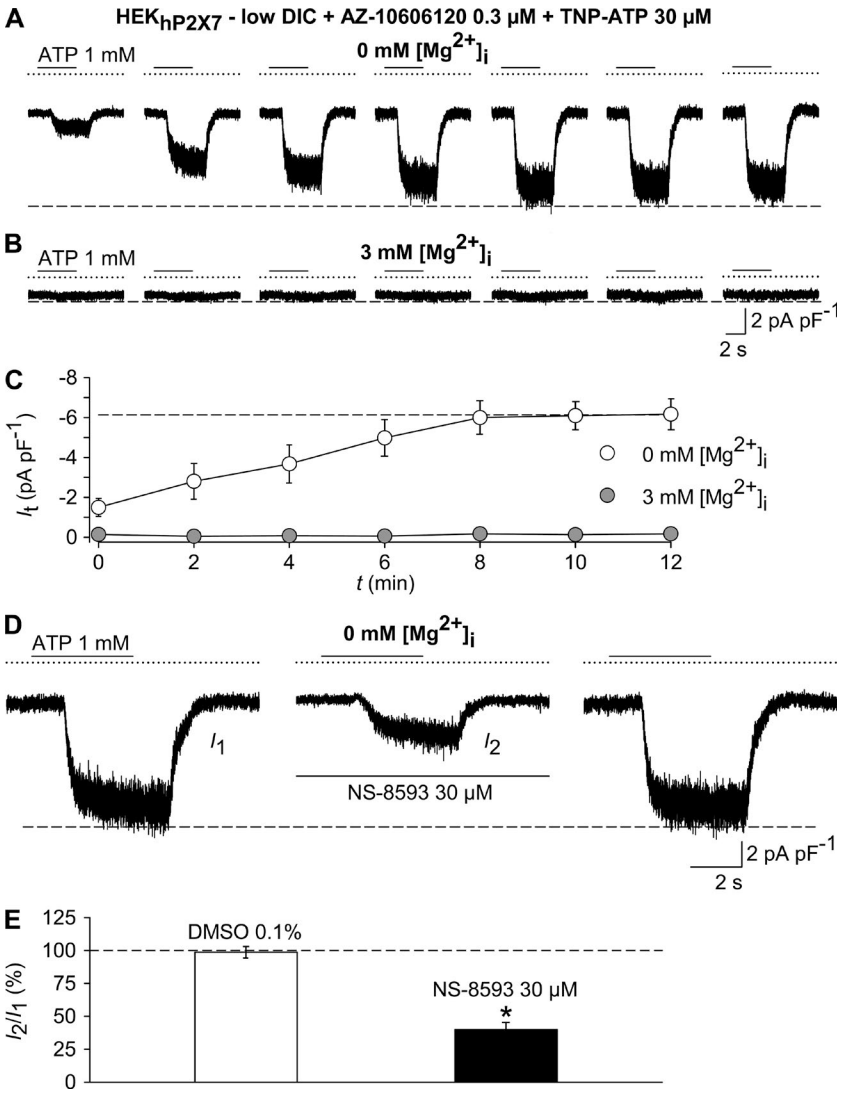

Figure 4. **ATP evokes TRPM7-like currents.** Whole-cell currents were recorded in HEK$_{hP2X7}$ cells in a low-DIC bath, using either Mg^{2+}-free or Mg^{2+}-containing (3 mM) pipette solutions. Cells were repetitively exposed to 1 mM ATP for 4 s at 120-s intervals in the continuous presence of 0.3 µM AZ-10606120 and 30 µM TNP-ATP to inhibit P2X receptors. (A and B) Representative currents in response to pulses of 1 mM ATP, recorded with Mg^{2+}-free (A) or Mg^{2+}-containing (B) pipette solutions. (C) Statistical evaluation of 11 experiments each, performed as in A and B. Note that intracellular Mg^{2+} (gray circles) blunted responses to ATP. (D) Preconditioned (not depicted) TRPM7-like currents evoked by 1 mM ATP (left, I_1), 6 min after adding the TRPM7 modulator NS-8593 (30 µM; middle, I_2), and 6 min after removal of the blocker (right). (E) Statistical analysis of experiments similar to those in D (n = 6–7 each). Peak currents in the presence of test compounds I_2 are shown normalized with respect to the pre-application peak current I_1. *, P < 0.001, significant difference from the DMSO control. In electrophysiological figures, dotted lines indicate the zero current level. Error bars indicate SEM.

induced channel activity shares the voltage dependence of Ca^{2+} to preferentially block the TRPM7-like conductance in excised patches at negative potentials. At positive potentials, both the fast block (reflected by the apparently reduced single channel conductance) and the slower, flickering block (reflected by shortening of mean open times) were overcome (Fig. S2), indicating that $[Ca^{2+}]_o$ impedes TRPM7 activity by binding within the electrical field of the membrane. Because $[Ca^{2+}]_o$ clamped to 2.4 µM mimicked the effect of extracellular ATP in low-DIC solutions, our conclusion is that partial activation of TRPM7 by releasing it from a Ca^{2+}-dependent block is the most likely molecular candidate to mediate sustained nonselective cation currents under conditions that are frequently applied to measure P2X7 channels. Finally, to confirm that dis-inhibition by low $[Ca^{2+}]_o$ of TRPM7-like single channel activity is responsible for global currents seen in the whole-cell mode upon lowering $[Ca^{2+}]_o$, we performed siRNA-mediated knockdown of TRPM7 expression, which resulted in a significant inhibition of no-DIC–induced whole-cell currents in HEK$_{hP2X7}$ cells compared with untransfected or control siRNA– or P2X7 siRNA–transfected cells (Fig. S3).

Strategies to avoid TRPM7-like channel coactivation while assaying P2X7

The strong enhancement of P2X7 currents in low-DIC solutions prompts researchers to use such conditions during electrophysiological recordings of P2X7 receptor activation. If more physiological DIC concentrations are contained in the bath solution, TRPM7 coactivation is disfavored. Nonetheless, it should be noted that ATP concentrations ≥1 mM evoke TRPM7-like currents also in a standard DIC bath (Fig. S4). Although these currents are much smaller compared with those in no-DIC solutions, P2X7 currents would also become tinier, and the concentration-response curve for ATP is shifted to higher ATP concentrations, thereby increasing DIC-chelating capacity.

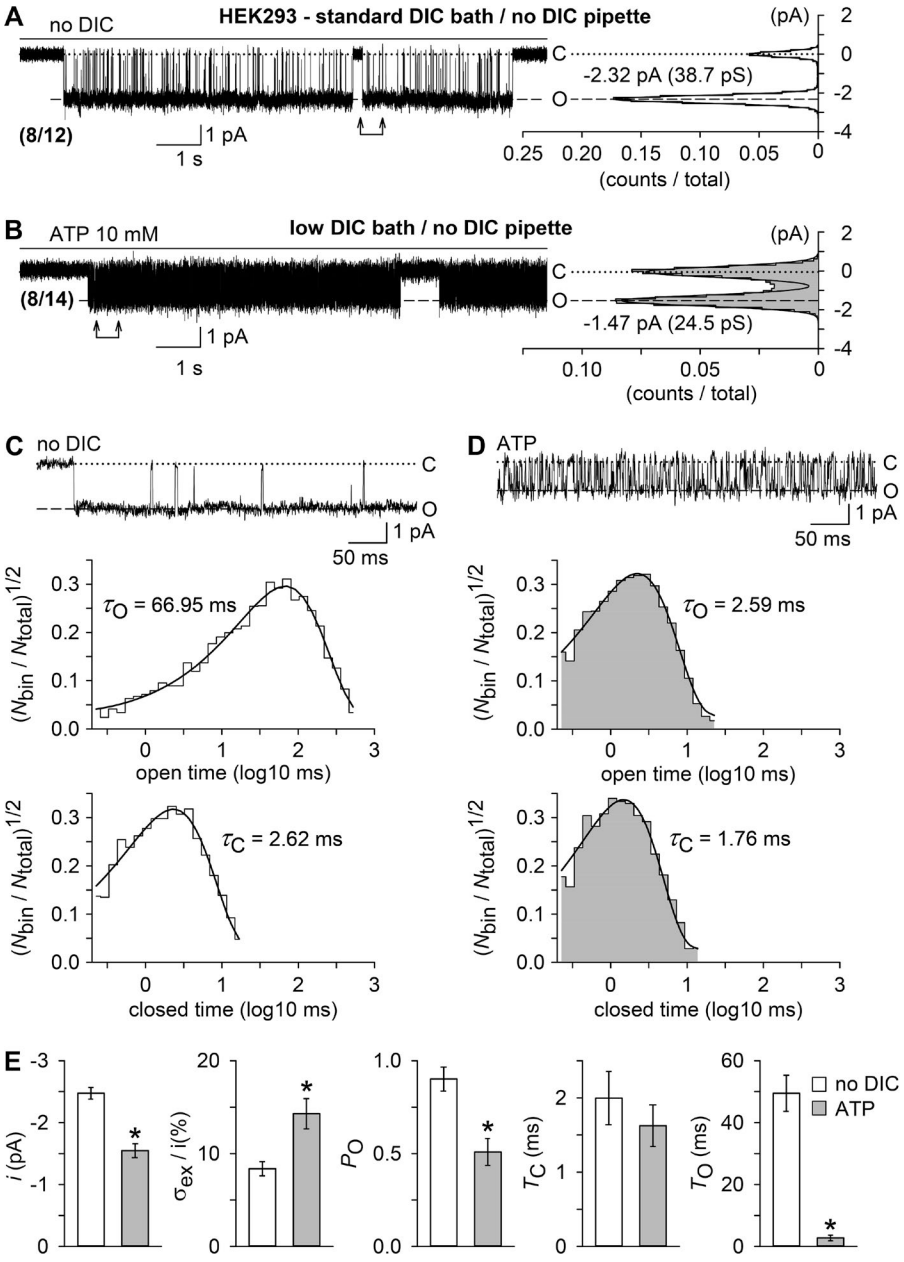

Figure 5. **Unitary currents evoked by a DIC-free bath solution (no DIC) or by ATP in outside-out patches.** Outside-out membrane patches were excised from parental HEK293 cells in standard DIC bath and no-DIC pipette solutions. (A and B) Examples of single channel currents, shown to the left, and respective all-point histograms (0.1 pA/bin) with superimposed Gaussian distributions, shown to the right, recorded in the absence of DICs (no DIC, 0 μM $[Ca^{2+}]_o$; A) or ATP (10 mM, 2.4 μM $[Ca^{2+}]_o$; B). Numbers in parentheses give the fraction of patches that responded with single open levels to either treatment. Inward currents are shown as downward deflections, and "C" and "O" indicate the closed and open level. The vertical axis in the histograms (current level, pA) has the same scale as the current traces, and the horizontal axis, the fractional point count (counts/total), includes 453 and 4,147 dwells from the 12-s data epochs in A and B, respectively. (C and D) The top panels show, at a higher time resolution, unitary current activity from the data sections specified by arrows in A and B. Note the smaller current amplitudes and a flickering behavior of channels in the presence of ATP (D). The bottom panels illustrate, from top to bottom, open and closed time histograms (~10 bins/decade) in the presence of no DIC (C) or ATP (D, gray shading), derived from idealization of recordings as shown in A and B but cumulated from multiple bursts of activity (C, 3,521 dwells in 12 bursts; D, 19,962 dwells in 5 bursts). Displayed is the square root–transformed ratio of the number of events per bin to the total number of events $((N_{bin}/N_{total})^{1/2})$ versus the logarithm of the bin width (log10 ms). Overlaying continuous black curves in the histograms represent probability density distributions. Respective opening (τ_O) and closing time constants (τ_C) are indicated. Note that distributions were seemingly single-peaked. (E) Statistical analysis of experiments similar to those in A and B (n = 8 each), showing, from left to right, unitary current amplitudes (i), relative excess open channel noise levels (σ_{ex}/ i) and intraburst open probabilities (P_O) of the channels activated by no DIC (open bars) or ATP (filled bars), derived from all-point histograms, as well as mean intraburst closed (T_C) and open times (T_O), derived from data idealization. *, P < 0.001, significantly different from the channel activity evoked by no DIC. In electrophysiological figures, dotted lines indicate the zero current level. Error bars indicate SEM.

Therefore, our data imply that alternative strategies should be used to prevent a coactivation of the ubiquitously expressed TRPM7. Because the pharmacological inhibitor waixenicin (Zierler et al., 2011) is not readily available, the inclusion of 1–5-mM concentrations of Mg^{2+} in the pipette solution is expected to reliably suppress TRPM7. In HEK_{hP2X7} cells that were intracellularly perfused with Mg^{2+}, current densities were ~30% smaller than in cells that were recorded with a Mg^{2+}-free intracellular solution (Fig. 7 A). When recorded with a Mg^{2+}-free pipette solution, addition of established competitive or noncompetitive P2X7 receptor antagonists AZ-10606120 (0.3 μM), A-438079 (10 μM), and A-839977 (1 μM) to the bath solution only partially suppressed 1 mM ATP–induced currents with a remaining current of ~20–25% (Fig. 7, B and D). In contrast, ATP-induced inward currents were abolished when HEK_{hP2X7} cells were intracellularly

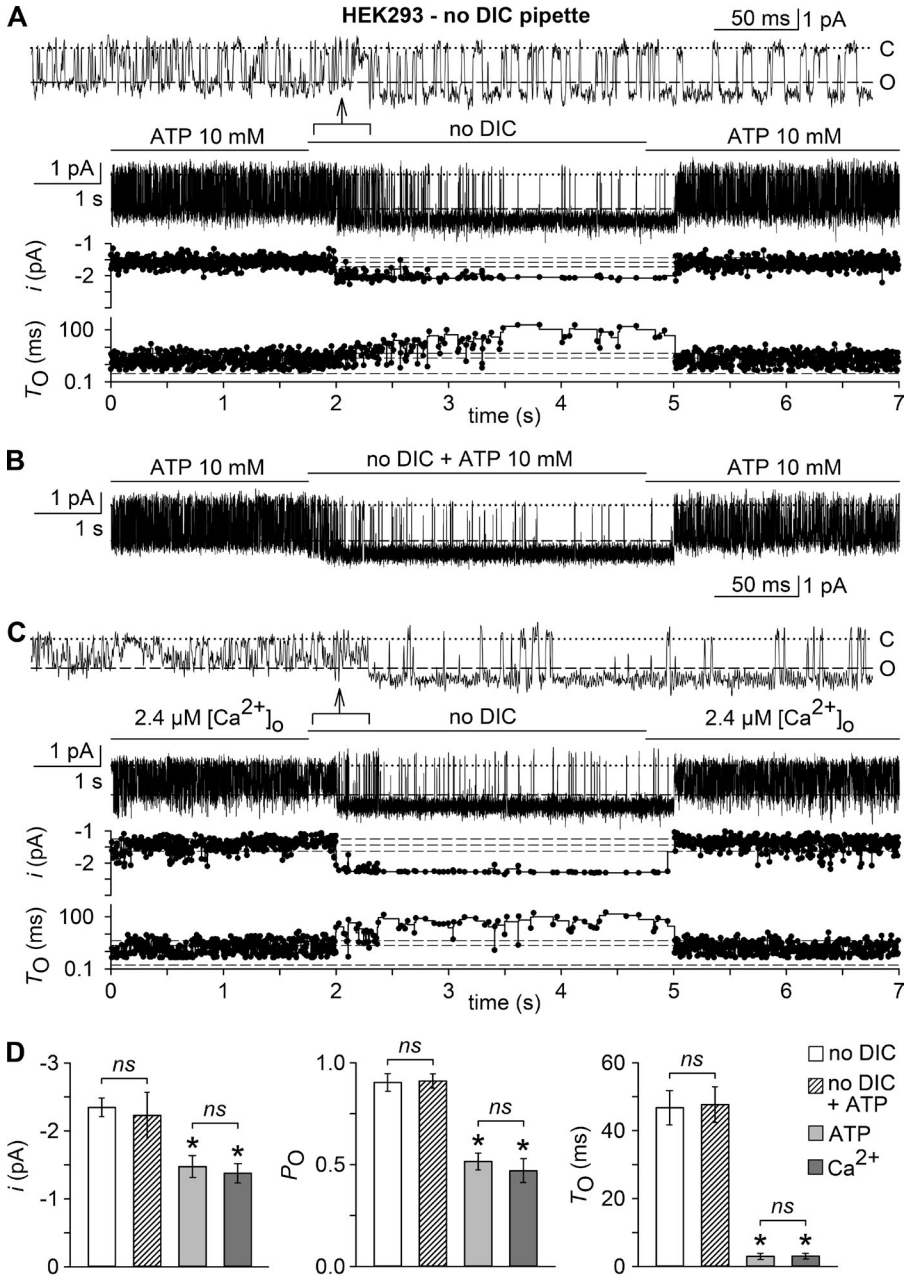

Figure 6. **Extracellular Ca^{2+} but not ATP apparently blocks TRPM7.** (A–C) Shown are currents in outside-out membrane patches excised with a pipette containing no-DIC solution from HEK293 cells. Currents were evoked either by low DIC plus 10 mM ATP (2.4 µM free $[Ca^{2+}]_o$; A and B) or by a bath solution containing only 2.4 µM free $[Ca^{2+}]_o$ (C). Channel activity was then modulated by switching to no DIC, without (A and C) or with added ATP (10 mM; B). Top panels in A and C show unitary current activity at a higher time resolution from the data sections specified by arrows. Bottom panels in A and C illustrate stability plots of unitary current amplitudes (*i*) and open times (T_O), when plotted versus time on the same abscissa scaling as the respective current traces. Broken lines indicate the mean and standard deviation of *i* or T_O during the 1.75 s of recording before the bath medium was exchanged. (D) Means ± SEM of unitary current amplitudes (*i*), intraburst open probabilities (P_O), mean intraburst closed times (T_C), and mean intraburst open times (T_O) of the channels activated by no DIC (open bars), no DIC plus 10 mM ATP (hatched bars), ATP (in low DIC; 2.4 µM free $[Ca^{2+}]_o$; light gray bars), and 2.4 µM $[Ca^{2+}]_o$ (dark gray bars). *, $P < 0.001$, significantly different from the channel activity evoked by no DIC; *ns*, not statistically significant; $n = 7–9$ each. Single channel parameters were derived from a 1.75-s recording period before bath exchange (ATP in low DIC, 2.4 µM $[Ca^{2+}]_o$) or from the last 2.5 s in no DIC and ATP in no DIC, respectively, and included 65–983 dwells. In electrophysiological figures, dotted lines indicate the zero current level.

perfused with 3 mM Mg^{2+} and then stimulated with 1 mM ATP (Fig. 7, C and D). Thus, contaminating TRPM7-like currents may cause an underestimation of antagonist efficacy. Although the apparent antagonist-resistant fraction already amounted 20–25% in the strongly P2X7-expressing stable cell line, it can be substantially larger in cells that natively express low physiological levels of P2X7, such as macrophages or astrocytes (Nörenberg et al., 2012). A possible drawback of the intracellular availability of Mg^{2+} is that numerous signaling cascades, including ATP-induced P2Y receptor activation and downstream signaling via Mg^{2+}-GTP–dependent heterotrimeric G proteins may cause regulation of various other ion channel families that may overlap with the observed P2X7 currents.

ATP activates TRPM7-like currents but not P2X7 currents in rat C6 glioma cells

We finally asked whether dis-inhibition of TRPM7 by millimolar ATP concentrations might have contributed to the assumption of functional expression of P2X7 in cells that endogenously express substantial amounts of TRPM7. We selected rat C6 glioma cells as an example for which P2X7 expression has been reported (Wei et al., 2008; Ryu et al., 2011). Like in parental HEK293 cells, addition of concentrations of ATP (1.25 or 5 mM) that reliably activate P2X7 failed to induce a P2X7-typical, long-lasting increase in $[Ca^{2+}]_i$ in C6 glioma cells (Fig. 8, A and B). Of note, a lower signal peak was consistently observed in HEK_{hP2X7} cells stimulated with 5 mM ATP compared with 1.25 mM ATP (Fig. 8 B). Be-

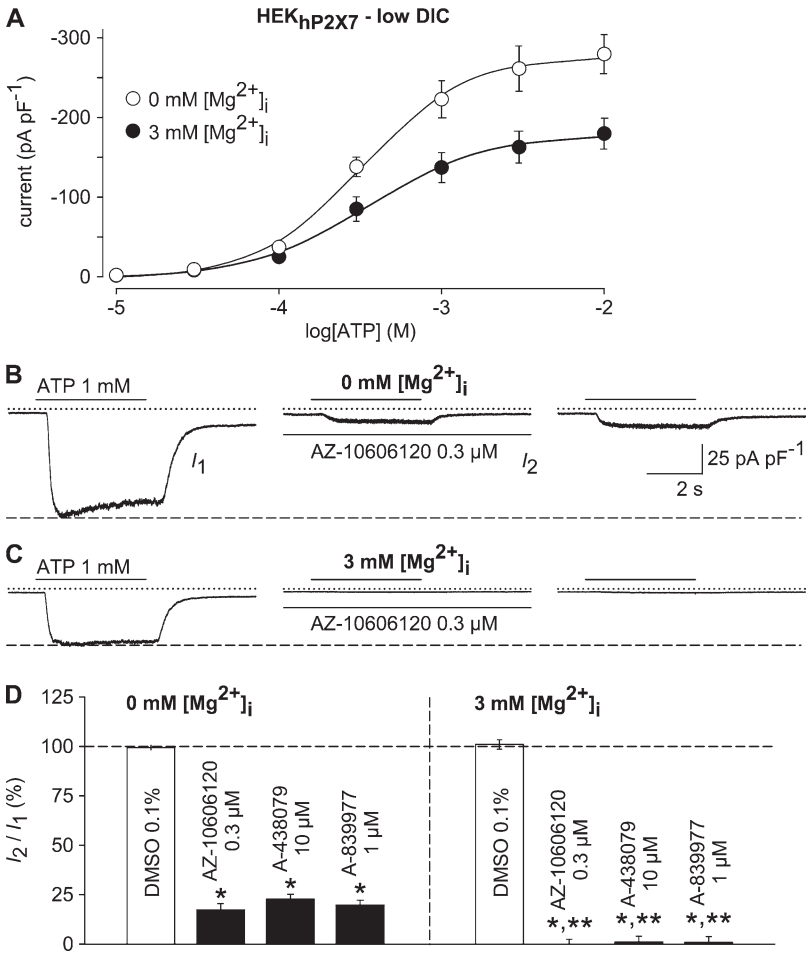

Figure 7. **Impact of TRPM7 coactivation on hP2X7 pharmacology.** (A) ATP concentration-response curves were constructed as in Fig. 1 (G–J) and obtained in the absence (open circles) and presence of 3 mM intracellular Mg^{2+} (filled circles; n = 11 each). Note the ~30% smaller responses to ATP when TRPM7 was blocked by internal Mg^{2+}. (B and C) 1 mM ATP–induced currents, obtained with a Mg^{2+}-free (B) or a Mg^{2+}-containing (3 mM) pipette solution (C), were recorded before (left, I_1), 6 min after the addition of AZ-10606120 (0.3 µM; middle, I_2), and 6 min after removal of the compound (right). (D) Statistical analysis of experiments performed as outlined in B (left, 0 mM [Mg^{2+}]$_i$) and C (right, 3 mM [Mg^{2+}]$_i$; n = 9–11 each). ATP-induced peak currents in the presence of 0.3 µM AZ-10606120, 10 µM A-438079, or 1 µM A-839977 were normalized to the respective pre-application peak currents (I_1). Significant differences to the DMSO controls (*, $P < 0.001$) and significant differences to the respective drug effects obtained with 0 mM [Mg^{2+}]$_i$ (**, $P < 0.001$) are depicted. Recordings were performed in low-DIC bath after current run-up in response to repetitive stimulation with 1 mM ATP was completed (not depicted). In electrophysiological figures, dotted lines indicate the zero current level. Error bars indicate SEM.

cause a bell-shaped concentration response curve is not reported for P2X7 currents, this effect is most likely caused by a lower availability of free extracellular Ca^{2+} in the presence of excess amounts of ATP. An ATP-induced transient increase in $[Ca^{2+}]_i$ was seen in the glioma cells (Fig. 8 A) but not significantly affected by the P2X7-selective antagonist AZ10606120 (100 nM). Similarly, Yo-Pro-1 uptake was not detectable in ATP-stimulated C6 glioma cells but clearly present in HEK$_{hP2X7}$ cells (Fig. 8 C). Western blot analysis confirmed the presence of TRPM7 in C6 glioma cells (Fig. 3 C), whereas no P2X7 expression was detected despite species cross-reactivity of the antibody (Fig. 8 D).

Whole-cell currents that were detected with a Mg^{2+}-free pipette solution in C6 glioma cells challenged with 10 mM ATP in a low-DIC solution showed a noninactivating inward current (at −60 mV) and an amplitude run-up during repeated stimulation (Fig. 9, A and C). As judged from their reversal potential (−2.8 ± 3.4 mV; n = 7), these currents were conducted by nonselective cation channels. In contrast to P2X7 currents, the responses were not significantly inhibited by a combined addition of 30 µM TNP-ATP and 0.3 µM AZ-10606120 (Fig. 9, D and E) but abolished upon inclusion of 3 mM $MgCl_2$ in the pipette solution (Fig. 9, B and C). The finding of similar $[Mg^{2+}]_i$-inhibitable currents being evoked by superfusing C6 cells with no-DIC solution (Fig. 9, F–H) corroborates the notion that dis-inhibition of a nonselective cation channel from a DIC-dependent block rather than ATP binding to a channel target has mimicked the responses.

To ascertain that TRPM7 is the channel carrying the nonselective cation currents, we conducted a ramp protocol to activate TRPM7 in the same fashion as done in HEK$_{hP2X7}$ cells (Fig. 3 A). The outwardly rectifying currents converted to almost linear I/V relationship upon removal of extracellular DIC (Fig. 10, A and B), indicating functional expression of TRPM7. As expected, the no-DIC–evoked inward currents in C6 glioma cells were strongly inhibited by 30 µM NS-8593 but not by the P2X7-specific inhibitors AZ-10606120, A-438079, or A-839977 (Fig. 10, C, D, and G), which were applied at concentrations that are effective on P2X7 (Fig. 7 D).

Previously, beneficial effects of systemically administered BBG were observed in an experimental therapy model based on orthotopically implanted C6 glioblastoma and were attributed to a modulation of P2X7 (Ryu et al., 2011). In the light of our findings, we tested the impact of BBG on TRPM7-like currents in C6 glioma cells. Indeed, when applied at increas-

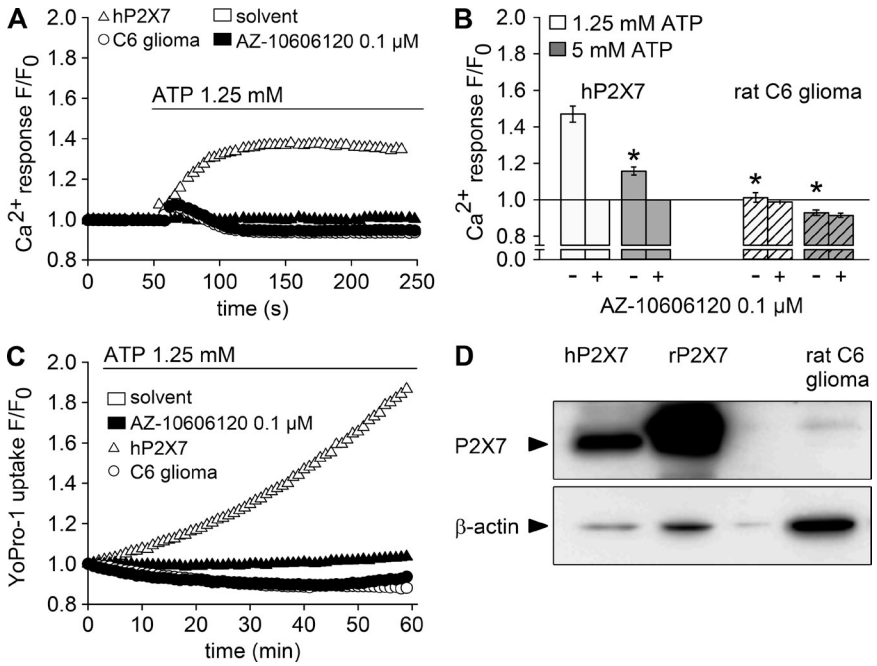

Figure 8. **Lack of functional P2X7 expression in rat C6 glioma cells.** HEK_{hP2X7} (triangles) and rat C6 glioma cells (circles) were subjected to Ca^{2+} and Yo-Pro-1 uptake assays and probed for P2X7 expression. (A) Fluo-4/AM–loaded cells were incubated with 0.1 µM AZ10606120 (filled symbols) or solvent (open symbols) for 5 min, and Fluo-4 fluorescence was detected before and after injection of 1.25 mM ATP as indicated. Fluorescence intensities (F) were normalized to the respective initial intensities (F_0), and representative examples for HEK_{hP2X7} and rat C6 glioma cells are shown. (B) Statistical analysis (means ± SEM) of four to five independent measurements performed as shown in A or with a higher ATP concentration (5 mM, gray bars). Asterisks indicate significant differences (*, $P < 0.05$) compared with HEK_{hP2X7} cells stimulated with 1.25 mM ATP. (C) Yo-Pro-1 fluorescence was measured in HEK_{hP2X7} and in C6 glioma cells in low-DIC buffer, containing 0.1 mM $CaCl_2$ and no $MgCl_2$, supplemented with 0.1 µM AZ10606120 or solvent 5 min before stimulation with 1.25 mM ATP. Shown are background-corrected fluorescence intensities normalized to the initial intensity (F_0). (D) Immunoblot analysis of P2X7 and β-actin in whole-cell lysates from HEK293 cells stably expressing human (hP2X7) or rat (rP2X7) P2X7 and from rat C6 glioma cells. Arrowheads indicate the expected molecular mass of human P2X7 (69 kD) and β-actin (42 kD).

ing concentrations, BBG exerted a complex interference with the TRPM7-like conductance. Although 100 nM BBG potentiated the no-DIC–induced inward currents, 1–10 µM BBG caused an ~50% inhibition of the TRPM7-like conductance (Fig. 10, E–G), indicating a possible involvement of TRPM7 in the previously observed effects.

DISCUSSION

The main finding of the present study was that extracellular ATP concentrations that are commonly applied to stimulate P2X7 receptors can evoke cellular responses, which are not mediated by a purinergic receptor. This noncanonical effect comprises the induction of a nonselective cation conductance, presumably by dis-inhibition of the ubiquitously expressed TRPM7 channel. The membrane currents had some properties that are commonly regarded as typical for P2X7, including the requirement of millimolar ATP concentrations for activation, inhibition by ambient DICs, a nonselective cation conductance with an almost linear I/V relationship at membrane potentials between −100 and 40 mV, and a gradual run-up of responses upon recurrent stimulation. Hence, some precautions should be taken to avoid misclassification of ATP responses by means of electrophysiological techniques. The analysis of additional features is suggested to distinguish the noncanonical ATP-induced TRPM7-like currents from those conducted by P2X7. These include the application of highly potent and selective P2X7 antagonists and the inhibition of TRPM7 by intracellular Mg^{2+}. Fluorometric $[Ca^{2+}]_i$ or Yo-Pro-1 uptake assay should be less prone to misjudgments because TRPM7 has been shown to possess only a limited Ca^{2+} permeability (Monteilh-Zoller et al., 2003) and has no discernable permeability for the organic cation Yo-Pro-1.

Receptor-independent, pleiotropic mode of action of extracellular ATP

In both cell models applied in this study, our data suggest a receptor-independent action of ATP. HEK293 cells have been shown to express at least P2X4 and P2X5 (Worthington et al., 1999), from which hP2X5 turned out to constitute a nonfunctional deletion mutant (Duckwitz et al., 2006), whereas rat C6 glioma cells may be endowed with P2X7 (Wei et al., 2008). All known functional P2X receptor subtypes are, however, suscep-

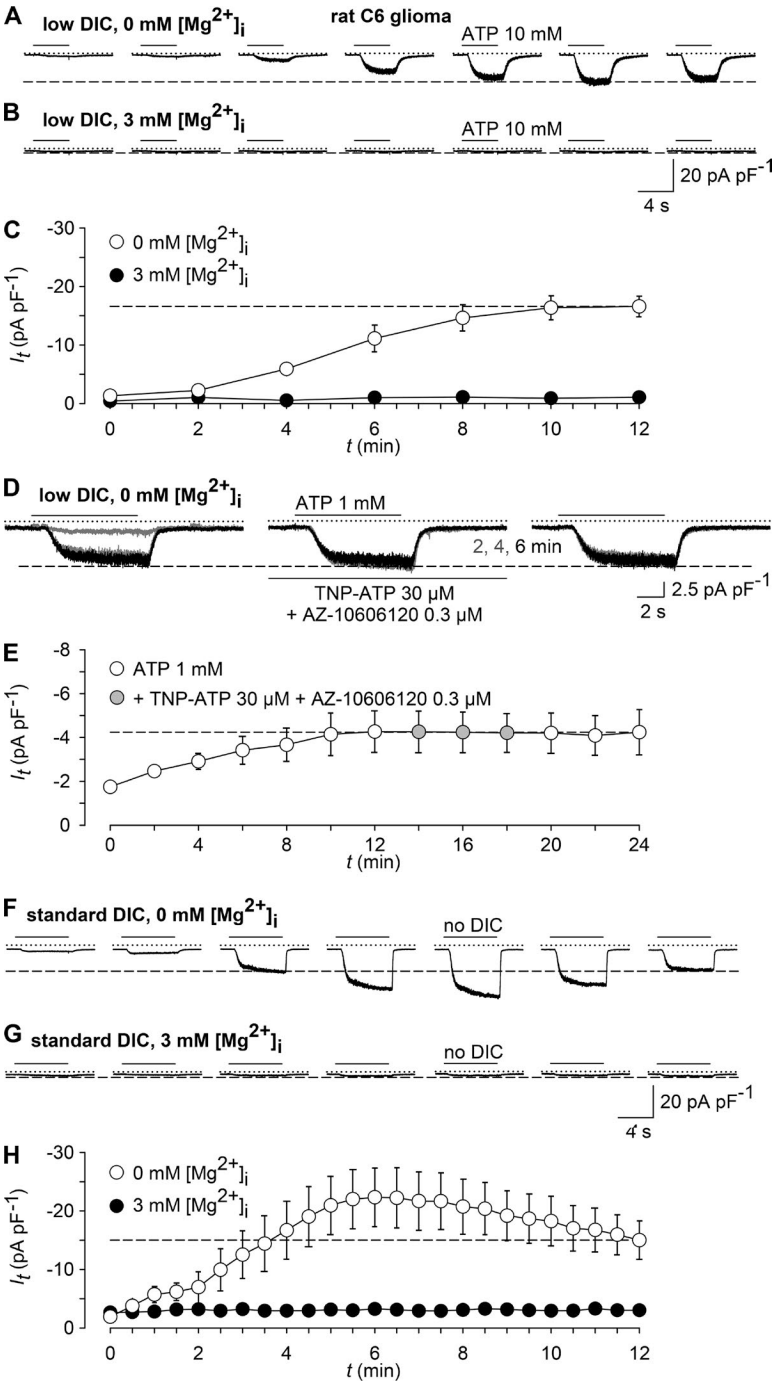

Figure 9. **ATP evokes TRPM7-like currents but no P2X7 activity in rat C6 glioma cells.** (A and B) Shown are whole-cell currents evoked by repetitive (4 s at 120-s intervals) application of 10 mM ATP in rat C6 glioma cells, when recording with a Mg^{2+}-free (A) or 3 mM Mg^{2+}–containing pipette solution (B). (C) Statistical evaluation of experiments similar to those in A (open circles) and B (filled circles; $n = 8$ each). (D) Shown are superimposed whole-cell currents in response to 1 mM ATP during preconditioning (left), after 2, 4, and 6 min in the presence of 30 µM TNP-ATP plus 0.3 µM AZ-10606120 (middle), and 2, 4, and 6 min after removal of the P2X antagonists (right). (E) Data accumulated from seven experiments as in D. Note the lack of effect of P2X receptor blockade. (F–H) Functional detection of TRPM7-like currents in C6 glioma cells. (F and G) TRPM7-like currents evoked by repetitive (6 s at 30-s intervals) application of no-DIC bath solution in cells internally perfused with a Mg^{2+}-free (F) or 3 mM Mg^{2+}–containing pipette solution (G). (H) Statistical evaluation of experiments similar to those in F (open circles) and G (filled circles; $n = 8$ and 6). Note that intracellular Mg^{2+} equally abolished the responses to ATP (C) and to the no-DIC bath (H). In electrophysiological figures, dotted lines indicate the zero current level. Error bars indicate SEM.

tible to the inhibitory effects of either TNP-ATP or AZ-10606120 (Jarvis and Khakh, 2009; Coddou et al., 2011). Because the noncanonical currents evoked by ATP in both tumor cell lines were not affected by a mixture of these antagonists, they were decisively not conducted by P2X receptor channels. This view is strongly supported by the failure to perceive ATP-induced changes in $[Ca^{2+}]_i$ or in Yo-Pro-1 uptake and by single channel properties that are incompatible with those of P2X7.

The P2X4 protein described in HEK293 cells (Worthington et al., 1999) was thus apparently not assembled into functional channel complexes or, if they were so, not targeted to the cell membrane. Accordingly, P2X4 is known to be largely compartmentalized within cytoplasmic structures such as vesicles, vacuoles, lamellar bodies, and lysosomes (Xu et al., 2014). With respect to the proposed presence of P2X7 in rat glioma (Wei et al., 2008), we could, however, not detect the respective protein. The rat C6 cells of this previous study were used after unusually high cell passage numbers (39–59 times; Wei et al., 2008), during which they may have gained astrocyte-like properties (Mangoura et al.,

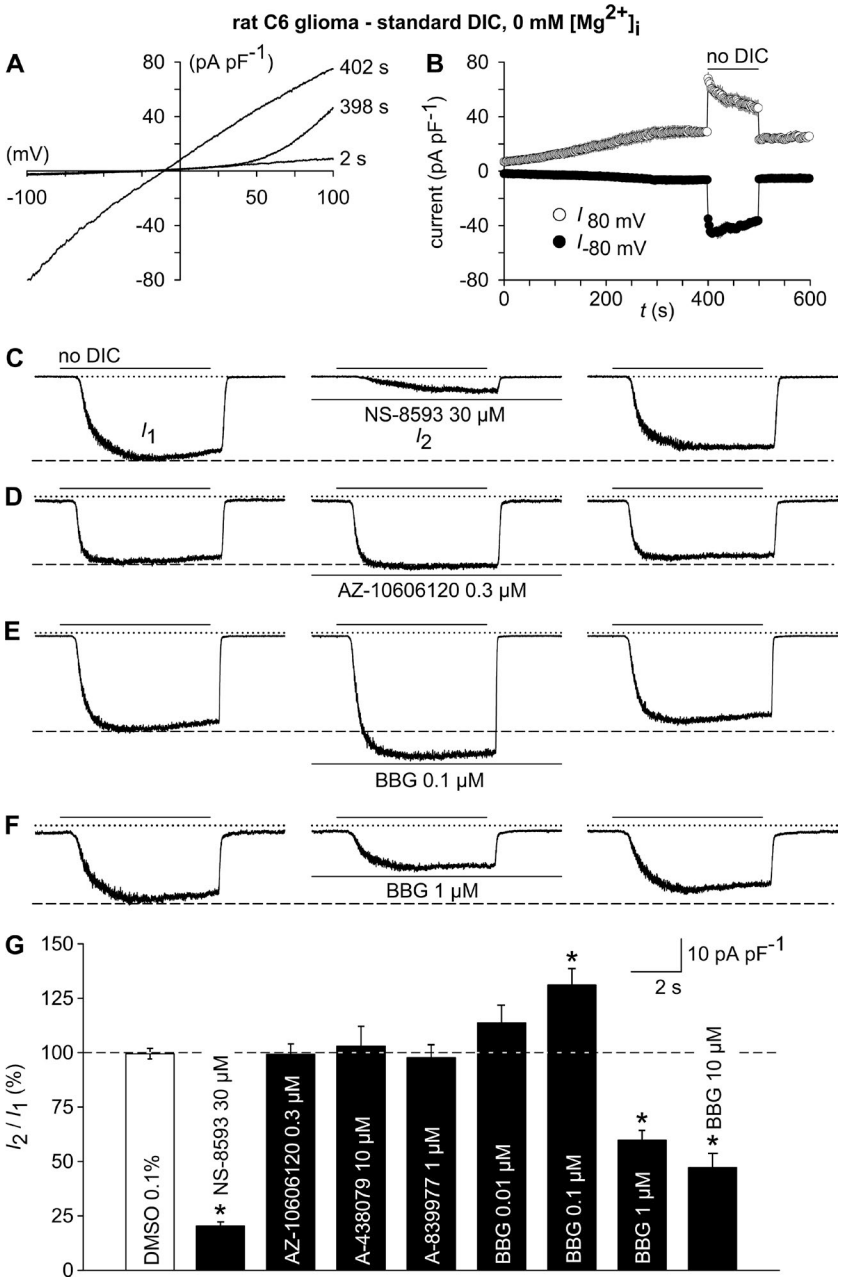

Figure 10. **Electrophysiological TRPM7 fingerprint and effects of P2X7 receptor antagonist on TRPM7-like currents in rat C6 glioma cells.** (A) Whole-cell currents were measured during repetitive (every 2 s) application of voltage ramps (−100 to 100 mV; 0.8 mV/ms) under standard DIC conditions at 2 and 398 s after the start of the experiment and after switching to a no-DIC bath solution (402 s). (B) Statistical evaluation of seven experiments performed as in A. Shown are inward current amplitudes at −80 mV (filled circles) and outward current amplitudes at 80 mV (open circles) versus time. (C–F) TRPM7-like whole-cell currents at −60 mV, recorded after preconditioning (not depicted), were elicited by repetitive exposure (6 s at 30-s intervals) to no DIC before (left; I_1) and 6 min after exposure to the indicated TRPM7 and P2X modulators (middle; I_2). (right) Currents 6 min after wash-out of the test compounds. (G) Statistical analysis of experiments as in A–E (n = 7–9 each). TRPM7-like peak currents in the presence of the test compounds (I_2) are normalized to the respective pre-application peak currents (I_1). *, P < 0.001, significantly different from the control condition (DMSO). In electrophysiological figures, dotted lines indicate the zero current level. Error bars indicate SEM.

1989), and rat cultured astrocytes were in fact endowed with functional P2X7 receptors (Nörenberg et al., 2010).

Previous studies have described functional P2Y subtypes in HEK293 (Schachter et al., 1997) and rat C6 glioma cells (Sabała et al., 2001; Van Kolen and Slegers, 2004). However, metabotropic receptors were definitely not implicated in the activation of the atypical ATP responses. The latter could not only be elicited in the absence of intracellular Mg^{2+}, i.e., when an indispensable prerequisite for GDP/GTP exchange and therefore for G protein–dependent signaling was lacking (Birnbaumer, 2007), but were in fact abolished by its substitution. Also, ATP effects on endogenous $P2Y_1$ and $P2Y_2$ receptors expressed in HEK293 cells require markedly lower agonist concentrations (Schachter et al., 1997) than the development of nonselective cation currents seen in this study.

Mechanism of the noncanonical ATP effect

The P2 receptor–independent biological effect of ATP was closely mimicked by further reducing the extracellular Ca^{2+} concentration, suggesting that the Ca^{2+}- and Mg^{2+}-buffering capability of ATP was causing dis-inhibition of a DIC-inhibited channel. Accordingly, we found that acute lowering of $[Ca^{2+}]_o$ was sufficient to trigger membrane current responses. Depending on the cell type, two different types of conductivity were found.

One type, a nondesensitizing current, closely mimicked the noncanonical ATP currents in HEK293 and in rat C6 glioma cells. The other response type was only seen in HEK293 cells. It comprised a rapidly desensitizing Na^+ current with inwardly rectifying I/V relationship and was pharmacologically addressable with amiloride, suggesting that ASIC1a is the underlying molecular entity (Gunthorpe et al., 2001). However, ASIC1a was not activating during application of ATP because it was actually inhibited by ATP (see Fig. S1).

The cation conduit for the noncanonical ATP effect was found to be the constitutively active, but Mg^{2+}- and Ca^{2+}-inhibited TRPM7 channel, whose expression has already been described in HEK293 cells (Nadler et al., 2001; Chubanov et al., 2012). Extracellular Ca^{2+} or other DICs are permeant to some degree, but they strongly bind to the selectivity filter and thereby limit inward currents through the obstructed pore. Removal of extracellular DIC releases this permeation block, thereby changing the outwardly rectifying behavior of partially blocked TRPM7 to a linear current-voltage response (Nadler et al., 2001; Runnels et al., 2001; Kerschbaum et al., 2003; Monteilh-Zoller et al., 2003).

TRPM7 is tightly regulated by the intracellular concentration of Mg^{2+}, an effect that involves two separate binding sites, one for Mg-ATP within the inherent cytoplasmic kinase domain of the protein and another for free Mg^{2+} located within the channel moiety (Schmitz et al., 2003; Demeuse et al., 2006). There are several lines of evidence that the Mg^{2+}-inhibited TRPM7 is carrying the noncanonical ATP-induced currents, including the sensitivity to NS-8593, a published TRPM7-inhibiting compound (Chubanov et al., 2012), the absence of responses in recordings using Mg^{2+}-containing pipette solutions, and most strikingly, the single channel data, showing typical 40 pS channels (Li et al., 2006) under complete Ca^{2+} removal, which are converted to a somewhat smaller and flickering conductance in the presence of 2.4 µM Ca^{2+} irrespective of the presence or absence of ATP (Fig. 6). Finally, transfection of a TRPM7-targeting siRNA strongly attenuated the responses to no-DIC solutions. The impact of either extracellular ATP or direct lowering of Ca^{2+} on single channel properties was strongly voltage dependent. Thus, it may be explained by fast and slower binding/dissociation to negatively charged amino acids that experience the electrical field of the cell membrane. Indeed, negatively charged amino acids that align the selectivity filter in the pore-forming region of TRPM7 have been shown to critically regulate permeation of and inhibition by DICs (Mederos y Schnitzler et al., 2008; Numata and Okada, 2008). It should be noted that we found TRPM7 to be expressed in rat C6 glioma cells, making it likely that ATP-induced currents are indeed mediated by TRPM7 and not via P2X7.

TRPM6, the closest phylogenetic relative of TRPM7, is mainly expressed in the kidney, the intestine, and the testis and shares important regulatory properties with TRPM7. These include the chanzyme structure, as well as the regulation by intracellular Mg^{2+} and extracellular DICs (Chubanov and Gudermann, 2014). There is ongoing debate as to whether TRPM6 can form functional channels on its own (Chubanov and Gudermann, 2014). If coexpressed with TRPM7, TRPM6 can form functional heteromeric channel complexes (Chubanov et al., 2004; Li et al., 2006). Hence, TRPM6 or TRPM6-bearing heteromeric complexes may share the same indirect ATP-dependent mode of disinhibition from an extracellular block, thereby contributing to noncanonical ATP-induced currents in specific tissues.

Possible biological implications

We do not assume that the newly described pleiotropic mechanism is involved in the gross physiological regulation of TRPM7 (or TRPM6) channel activity, even though respective current responses could be evoked in the presence of standard levels of extracellular DICs. It may play a role, however, in injured tissues, where massive amounts of ATP can leak out from damaged cells into a restricted extracellular space. Accordingly, there is evidence showing that TRPM7 can promote the death of cortical and hippocampal neurons under conditions of glucose/oxygen deprivation or cerebral ischemia (e.g., Aarts et al., 2003; Wei et al., 2007). Interestingly, it has been proposed that TRPM7 may be activated by a decrease in extracellular DICs, possibly via GluN (NMDA) receptor hyperactivity (Wei et al., 2007). Our data suggest that extracellular ATP may contribute to TRPM7 disinhibition as well.

In contrast, malignant tumors are known to frequently develop diffuse necrotic foci upon vascular insults, which then may cause leakage of ATP (Di Virgilio, 2012) but also compromise TRPM7 gating control in tumor cells around the hypoxic area because the intracellular regulatory sites for Mg-ATP and Mg^{2+} synergistically impede channel activity (Demeuse et al., 2006). Paracrine effects of ATP on cancer growth may thus be mediated in principle by TRPM7 (Fleig and Chubanov, 2014) and P2X7 (Di Virgilio, 2012), which both have been shown to potentially promote tumor cell proliferation (Tani et al., 2007; Adinolfi et al., 2012) and invasiveness (Clark et al., 2006; Jelassi et al., 2011). With respect to gliomas, the P2X7 antagonist BBG has been shown to suppress tumor growth after the injection of rat C6 cells into the brain (Ryu et al., 2011). However, we and others (Supłat-Wypych et al., 2010) were unable to find any evidence for functional P2X7 (or other P2X) receptors in this tumor cell line. Because our data demonstrate that BBG also modulates TRPM7, one should consider that this and presumably more molecular targets may account for the observed antitumor properties of BBG.

ACKNOWLEDGMENTS

This work was supported by the Deutsche Forschungsgemeinschaft (DFG) within the framework of FOR748 (Scha 941/2-1) and TRR-SFB 152 (P18).

The authors declare no competing financial interests.

Kenton J. Swartz served as editor.

Submitted: 21 March 2016
Accepted: 20 April 2016

REFERENCES

Aarts, M., K. Iihara, W.L. Wei, Z.G. Xiong, M. Arundine, W. Cerwinski, J.F. MacDonald, and M. Tymianski. 2003. A key role for TRPM7 channels in anoxic neuronal death. *Cell.* 115:863–877. http://dx.doi.org/10.1016/S0092-8674(03)01017-1

Adinolfi, E., L. Raffaghello, A.L. Giuliani, L. Cavazzini, M. Capece, P. Chiozzi, G. Bianchi, G. Kroemer, V. Pistoia, and F. Di Virgilio. 2012. Expression of P2X7 receptor increases in vivo tumor growth. *Cancer Res.* 72:2957–2969. http://dx.doi.org/10.1158/0008-5472.CAN-11-1947

Babini, E., M. Paukert, H.S. Geisler, and S. Gründer. 2002. Alternative splicing and interaction with di- and polyvalent cations control the dynamic range of acid-sensing ion channel 1 (ASIC1). *J. Biol. Chem.* 277:41597–41603. http://dx.doi.org/10.1074/jbc.M205877200

Birnbaumer, L. 2007. Expansion of signal transduction by G proteins. The second 15 years or so: from 3 to 16 α subunits plus βγ dimers. *Biochim. Biophys. Acta.* 1768:772–793. http://dx.doi.org/10.1016/j.bbamem.2006.12.002

Chubanov, V., and T. Gudermann. 2014. TRPM6. *In* Mammalian transient receptor (TRP) cation channels. Vol. 222. B. Nilius, and V. Flockerzi, editors. Springer, Berlin, Heidelberg. 503–520. http://dx.doi.org/10.1007/978-3-642-54215-2_20

Chubanov, V., S. Waldegger, M. Mederos y Schnitzler, H. Vitzthum, M.C. Sassen, H.W. Seyberth, M. Konrad, and T. Gudermann. 2004. Disruption of TRPM6/TRPM7 complex formation by a mutation in the TRPM6 gene causes hypomagnesemia with secondary hypocalcemia. *Proc. Natl. Acad. Sci. USA.* 101:2894–2899. http://dx.doi.org/10.1073/pnas.0305252101

Chubanov, V., M. Mederos y Schnitzler, M. Meißner, S. Schäfer, K. Abstiens, T. Hofmann, and T. Gudermann. 2012. Natural and synthetic modulators of SK ($K_{ca}2$) potassium channels inhibit magnesium-dependent activity of the kinase-coupled cation channel TRPM7. *Br. J. Pharmacol.* 166:1357–1376. http://dx.doi.org/10.1111/j.1476-5381.2012.01855.x

Clark, K., M. Langeslag, B. van Leeuwen, L. Ran, A.G. Ryazanov, C.G. Figdor, W.H. Moolenaar, K. Jalink, and F.N. van Leeuwen. 2006. TRPM7, a novel regulator of actomyosin contractility and cell adhesion. *EMBO J.* 25:290–301. http://dx.doi.org/10.1038/sj.emboj.7600931

Coddou, C., Z. Yan, T. Obsil, J.P. Huidobro-Toro, and S.S. Stojilkovic. 2011. Activation and regulation of purinergic P2X receptor channels. *Pharmacol. Rev.* 63:641–683. http://dx.doi.org/10.1124/pr.110.003129

Demeuse, P., R. Penner, and A. Fleig. 2006. TRPM7 channel is regulated by magnesium nucleotides via its kinase domain. *J. Gen. Physiol.* 127:421–434. http://dx.doi.org/10.1085/jgp.200509410

Di Virgilio, F. 2012. Purines, purinergic receptors, and cancer. *Cancer Res.* 72:5441–5447. http://dx.doi.org/10.1158/0008-5472.CAN-12-1600

Duckwitz, W., R. Hausmann, A. Aschrafi, and G. Schmalzing. 2006. $P2X_5$ subunit assembly requires scaffolding by the second transmembrane domain and a conserved aspartate. *J. Biol. Chem.* 281:39561–39572. http://dx.doi.org/10.1074/jbc.M606113200

Fleig, A., and V. Chubanov. 2014. TRPM7. *In* Mammalian transient receptor potential (TRP) cation channels. Vol. 222. B. Nilius, and V. Flockerzi, editors. Springer, Berlin, Heidelberg. 521–546. http://dx.doi.org/10.1007/978-3-642-54215-2_21

Gunthorpe, M.J., G.D. Smith, J.B. Davis, and A.D. Randall. 2001. Characterisation of a human acid-sensing ion channel (hASIC1a) endogenously expressed in HEK293 cells. *Pflugers Arch.* 442:668–674. http://dx.doi.org/10.1007/s004240100584

Jarvis, M.F., and B.S. Khakh. 2009. ATP-gated P2X cation-channels. *Neuropharmacology.* 56:208–215. http://dx.doi.org/10.1016/j.neuropharm.2008.06.067

Jelassi, B., A. Chantôme, F. Alcaraz-Pérez, A. Baroja-Mazo, M.L. Cayuela, P. Pelegrin, A. Surprenant, and S. Roger. 2011. $P2X_7$ receptor activation enhances SK3 channels- and cystein cathepsin-dependent cancer cells invasiveness. *Oncogene.* 30:2108–2122. http://dx.doi.org/10.1038/onc.2010.593

Kerschbaum, H.H., J.A. Kozak, and M.D. Cahalan. 2003. Polyvalent cations as permeant probes of MIC and TRPM7 pores. *Biophys. J.* 84:2293–2305. http://dx.doi.org/10.1016/S0006-3495(03)75035-8

Li, M., J. Jiang, and L. Yue. 2006. Functional characterization of homo- and heteromeric channel kinases TRPM6 and TRPM7. *J. Gen. Physiol.* 127:525–537. http://dx.doi.org/10.1085/jgp.200609502

Mangoura, D., N. Sakellaridis, J. Jones, and A. Vernadakis. 1989. Early and late passage C-6 glial cell growth: similarities with primary glial cells in culture. *Neurochem. Res.* 14:941–947. http://dx.doi.org/10.1007/BF00965927

Mederos y Schnitzler, M., J. Wäring, T. Gudermann, and V. Chubanov. 2008. Evolutionary determinants of divergent calcium selectivity of TRPM channels. *FASEB J.* 22:1540–1551. http://dx.doi.org/10.1096/fj.07-9694com

Monteilh-Zoller, M.K., M.C. Hermosura, M.J.S. Nadler, A.M. Scharenberg, R. Penner, and A. Fleig. 2003. TRPM7 provides an ion channel mechanism for cellular entry of trace metal ions. *J. Gen. Physiol.* 121:49–60. http://dx.doi.org/10.1085/jgp.20028740

Nadler, M.J., M.C. Hermosura, K. Inabe, A.L. Perraud, Q. Zhu, A.J. Stokes, T. Kurosaki, J.P. Kinet, R. Penner, A.M. Scharenberg, and A. Fleig. 2001. LTRPC7 is a Mg.ATP-regulated divalent cation channel required for cell viability. *Nature.* 411:590–595. http://dx.doi.org/10.1038/35079092

Nörenberg, W., J. Schunk, W. Fischer, H. Sobottka, T. Riedel, J.F. Oliveira, H. Franke, and P. Illes. 2010. Electrophysiological classification of P2X7 receptors in rat cultured neocortical astroglia. *Br. J. Pharmacol.* 160:1941–1952. http://dx.doi.org/10.1111/j.1476-5381.2010.00736.x

Nörenberg, W., H. Sobottka, C. Hempel, T. Plötz, W. Fischer, G. Schmalzing, and M. Schaefer. 2012. Positive allosteric modulation by ivermectin of human but not murine P2X7 receptors. *Br. J. Pharmacol.* 167:48–66. http://dx.doi.org/10.1111/j.1476-5381.2012.01987.x

Numata, T., and Y. Okada. 2008. Molecular determinants of sensitivity and conductivity of human TRPM7 to Mg^{2+} and Ca^{2+}. *Channels (Austin).* 2:283–286. http://dx.doi.org/10.4161/chan.2.4.6695

Qin, F. 2004. Restoration of single-channel currents using the segmental k-means method based on hidden Markov modeling. *Biophys. J.* 86:1488–1501. http://dx.doi.org/10.1016/S0006-3495(04)74217-4

Riedel, T., I. Lozinsky, G. Schmalzing, and F. Markwardt. 2007. Kinetics of $P2X_7$ receptor-operated single channels currents.

Biophys. J. 92:2377–2391. http://dx.doi.org/10.1529/biophysj.106.091413

Runnels, L.W., L. Yue, and D.E. Clapham. 2001. TRP-PLIK, a bifunctional protein with kinase and ion channel activities. *Science.* 291:1043–1047. http://dx.doi.org/10.1126/science.1058519

Ryu, J.K., N. Jantaratnotai, M.C. Serrano-Perez, P.L. McGeer, and J.G. McLarnon. 2011. Block of purinergic $P2X_7R$ inhibits tumor growth in a C6 glioma brain tumor animal model. *J. Neuropathol. Exp. Neurol.* 70:13–22. http://dx.doi.org/10.1097/NEN.0b013e318201d4d4

Sabała, P., R. Czajkowski, K. Przybyłek, K. Kalita, L. Kaczmarek, and J. Barańska. 2001. Two subtypes of G protein-coupled nucleotide receptors, $P2Y_1$ and $P2Y_2$ are involved in calcium signalling in glioma C6 cells. *Br. J. Pharmacol.* 132:393–402. http://dx.doi.org/10.1038/sj.bjp.0703843

Schachter, J.B., S.M. Sromek, R.A. Nicholas, and T.K. Harden. 1997. HEK293 human embryonic kidney cells endogenously express the $P2Y_1$ and $P2Y_2$ receptors. *Neuropharmacology.* 36:1181–1187. http://dx.doi.org/10.1016/S0028-3908(97)00138-X

Schmitz, C., A.L. Perraud, C.O. Johnson, K. Inabe, M.K. Smith, R. Penner, T. Kurosaki, A. Fleig, and A.M. Scharenberg. 2003. Regulation of vertebrate cellular Mg^{2+} homeostasis by TRPM7. *Cell.* 114:191–200. http://dx.doi.org/10.1016/S0092-8674(03)00556-7

Sherwood, T.W., E.N. Frey, and C.C. Askwith. 2012. Structure and activity of the acid-sensing ion channels. *Am. J. Physiol. Cell Physiol.* 303:C699–C710. http://dx.doi.org/10.1152/ajpcell.00188.2012

Sigworth, F.J., and S.M. Sine. 1987. Data transformations for improved display and fitting of single-channel dwell time histograms. *Biophys. J.* 52:1047–1054. http://dx.doi.org/10.1016/S0006-3495(87)83298-8

Supłat-Wypych, D., A. Dygas, and J. Barańska. 2010. 2′, 3′-*O*-(4-benzoylbenzoyl)-ATP-mediated calcium signaling in rat glioma C6 cells: role of the $P2Y_2$ nucleotide receptor. *Purinergic Signal.* 6:317–325. http://dx.doi.org/10.1007/s11302-010-9194-7

Tani, D., M.K. Monteilh-Zoller, A. Fleig, and R. Penner. 2007. Cell cycle-dependent regulation of store-operated I_{CRAC} and Mg^{2+}-nucleotide-regulated MagNuM (TRPM7) currents. *Cell Calcium.* 41:249–260. http://dx.doi.org/10.1016/j.ceca.2006.07.004

Van Kolen, K., and H. Slegers. 2004. $P2Y_{12}$ receptor stimulation inhibits β-adrenergic receptor-induced differentiation by reversing the cyclic AMP-dependent inhibition of protein kinase B. *J. Neurochem.* 89:442–453. http://dx.doi.org/10.1111/j.1471-4159.2004.02339.x

von Kügelgen, I., and T.K. Harden. 2011. Molecular pharmacology, physiology, and structure of the P2Y receptors. *Adv. Pharmacol.* 61:373–415. http://dx.doi.org/10.1016/B978-0-12-385526-8.00012-6

Wei, W.L., H.S. Sun, M.E. Olah, X. Sun, E. Czerwinska, W. Czerwinski, Y. Mori, B.A. Orser, Z.G. Xiong, M.F. Jackson, et al. 2007. TRPM7 channels in hippocampal neurons detect levels of extracellular divalent cations. *Proc. Natl. Acad. Sci. USA.* 104:16323–16328. http://dx.doi.org/10.1073/pnas.0701149104

Wei, W., J.K. Ryu, H.B. Choi, and J.G. McLarnon. 2008. Expression and function of the $P2X_7$ receptor in rat C6 glioma cells. *Cancer Lett.* 260:79–87. http://dx.doi.org/10.1016/j.canlet.2007.10.025

Worthington, R.A., J.L. Dutton, P. Poronnik, M.R. Bennett, and J.A. Barden. 1999. Localisation of P_{2X} receptors in human salivary gland epithelial cells and human embryonic kidney cells by sodium dodecyl sulfate-polyacrylamide gel electrophoresis/Western blotting and immunofluorescence. *Electrophoresis.* 20:2065–2070. http://dx.doi.org/10.1002/(SICI)1522-2683(19990701)20:10<2065::AID-ELPS2065>3.0.CO;2-E

Xu, J., H. Chai, K. Ehinger, T.M. Egan, R. Srinivasan, M. Frick, and B.S. Khakh. 2014. Imaging P2X4 receptor subcellular distribution, trafficking, and regulation using P2X4-pHluorin. *J. Gen. Physiol.* 144:81–104. http://dx.doi.org/10.1085/jgp.201411169

Yan, Z., A. Khadra, A. Sherman, and S.S. Stojilkovic. 2011. Calcium-dependent block of P2X7 receptor channel function is allosteric. *J. Gen. Physiol.* 138:437–452. http://dx.doi.org/10.1085/jgp.201110647

Zierler, S., G. Yao, Z. Zhang, W.C. Kuo, P. Pörzgen, R. Penner, F.D. Horgen, and A. Fleig. 2011. Waixenicin A inhibits cell proliferation through magnesium-dependent block of transient receptor potential melastatin 7 (TRPM7) channels. *J. Biol. Chem.* 286:39328–39335. http://dx.doi.org/10.1074/jbc.M111.264341